Infrared Study of the Pressure-Induced Isostructural Metallic Transition in Mo0.5W0.5S2

Infrared Study of the Pressure-Induced Isostructural Metallic Transition in $Mo_{0.5}W_{0.5}S_2$

Elena Stellino,[†] Francesca Ripanti,[*,‡] Giacomo Nisini,[‡] Francesco Capitani,[¶] Caterina Petrillo,[†] and Paolo Postorino[*,‡]

[†]*Department of Physics and Geology, University of Perugia, via Alessandro Pascoli, Perugia, Italy*

[‡]*Department of Physics, Sapienza University of Rome, P.le A. Moro 5, Rome, Italy*

[¶]*Synchrotron SOLEIL, LâĂŹOrme des Merisiers, Saint-Aubin, Gif-sur-Yvette, France*

E-mail: francesca.ripanti@uniroma1.it; paolo.postorino@roma1.infn.it

Abstract

Ternary compounds of Transition Metal Dichalcogenides are emerging as an interesting class of crystals with tunable electronic properties, which make them attractive for nano-electronic and optoelectronic applications. Among them, $Mo_xW_{1-x}S_2$ is one of the most studied alloys, due to the well-known, remarkable features of its binary constituents, MoS_2 and WS_2. The band-gap of this compound can be modelled varying Mo and W percentages in the sample, and its vibrational modes result from a combination of MoS_2 and WS_2 phonons. In this work, we report transmission measurements on a $Mo_{0.5}W_{0.5}S_2$ single crystal in the far-infrared range. Absorbance spectra collected at ambient conditions enabled, for the first time, a classification of the infrared-active phonons, complementary to Raman studies. High-pressure measurements allowed to study the evolution of both the lattice dynamics and the free carrier density up to 31 GPa, suggesting the occurrence of an isostructural semiconductor-to-metal transition

above 18 GPa, in very good agreement with the theoretical calculation reported in the literature.

Introduction

Among two-dimensional materials, in the last years, Transition Metal Dichalcogenides (TMDs) have proved to be one of the most promising classes of crystals in terms of both applications and fundamental studies. Semiconducting TMDs are characterized by a graphene-like layered lattice, easily exfoliable down to atomic-thick crystals,[1–3] but, at variance with graphene, their band structure exhibits finite band-gaps in the eV scale, which are attractive for electronic devices.[4–6] One of the most remarkable features of TMDs, as well as many others 2D materials, is the key role of the inter-layer interaction in determining the sample properties,[7–9] such as the strong relationship between the electronic structure and the number of layers. Indeed, in most semiconductors, a progressive increase of the band-gap is observed as the number of layers reduces, and an indirect-to-direct band-gap crossover arises when bilayer samples are scaled down to monolayers.[10–12]

Due to the high heterogeneity and the outstanding structural and electronic properties of isomorphic semiconducting TMDs, the possibility to design and produce heterostructures (formed by stacking together monolayers of different crystals) and alloys (synthesized by directly mixing two different TMDs) with different band-gaps has emerged as an appealing strategy to tune and tailor the band-structure of these materials for nano-electronic and optoelectronic applications. In this framework, ternary compounds have been synthesized where the metal or the chalcogen contributions are adjusted with different atoms from the same element group.[13,14]

$Mo_xW_{1-x}S_2$ is one of the most investigated TMD alloys, due to the vast amount of studies on its binary constituents MoS_2 and WS_2.[15–20] The bulk crystal shows a 2H phase and is formed by stacking together monolayer alloys via van der Waals interactions. The mono-

layer alloy contains one MoW plane sandwiched by two S planes, represented as S-Mo/W-S. Recent work on $Mo_xW_{1-x}S_2$ has proved that the electronic band-gap at ambient conditions can be tuned by modifying the percentage of Mo and W atoms in the lattice.[21,22] Raman measurements have also been performed, varying the number of layers and the stoichiometric composition, to characterize the vibrational modes of the sample.[23,24]

The application of pressure is a powerful tool to probe the inter-layer interactions in $Mo_xW_{1-x}S_2$ and to explore the tunability of the electronic and structural properties. Indeed, experimental and theoretical reports have already demonstrated that pressure can modulate the band structure of TMDs in general,[25,26] and, in particular, of MoS_2 and WS_2.[27–31] In MoS_2 a metallization has been observed at $\sim$ 19 GPa, accompanied by a structural distortion from $2H_c$ to $2H_a$ phase.[27,32] Similarly, in WS_2 a metallic transition occurs at $\sim$ 22 GPa, but, at variance with the previous case, the lattice remains isomorphic.[28] High-pressure Raman measurements on $Mo_{0.5}W_{0.5}S_2$ have suggested the absence of structural transitions up to 40 GPa.[33] Regarding the electronic properties, instead, in a recent article by Dong et al.[34] a semiconductor-to-metal transition has been predicted below 30 GPa for $Mo_{1-x}W_xS_2$ alloys through theoretical calculations. The metallization pressure was found to be dependent on both the number of layers and the Mo/W percentage in the sample. In particular, for bulk $Mo_{0.5}W_{0.5}S_2$ the authors suggested the onset of the transition above 20 GPa.

Here we report high-pressure transmission measurements on $Mo_{0.5}W_{0.5}S_2$ in the far-infrared (FIR) range, where simultaneous information on the lattice dynamics, complementary to Raman studies, and on the pressure-induced increase of the carrier density is accessible. This work classifies for the first time the infrared-active modes of $Mo_{0.5}W_{0.5}S_2$ at ambient conditions, analyzes their response under pressure, confirming the absence of structural transitions up to 31 GPa, and observes an abrupt increase of the carrier density above 18 GPa, associated to the onset of a semiconductor-to-metal transition.

Experimental

$Mo_{0.5}W_{0.5}S_2$, MoS_2, and WS_2 single crystals were provided by HQ-Graphene. All measurements were performed on fresh-cut samples, directly cleaved from the macroscopic crystal to obtain flakes a few microns thick with a clean surface. It is worth noticing that, since the typical thickness of single-layer TMDs is ~ 0.7 nm, in the present case we safely work in the bulk limit.

Room temperature infrared transmission measurements were performed at the beamline SMIS of the SOLEIL synchrotron both at ambient pressure (on all the samples) and over the $0 \div 30$ GPa range (only on $Mo_{0.5}W_{0.5}S_2$).

In the DAC (orange), diamonds with a culet of 250 μm^2 were separated by a pre-indented stainless steel 50 μm thick gasket, in which a hole of 125 μm diameter was drilled. The exfoliated sample was positioned in the hole together with CsI as pressure transmitting medium[35] and a ruby chip, to measure the pressure through the ruby fluorescence technique.[36] The measured sample was 50 μm^2 in area and 2-3 μm in thickness.

Measurements were performed using a Thermo Fisher iS50 interferometer equipped with a solid-substrate beamsplitter. Synchrotron edge radiation was employed as light source. Custom-made 15x Cassegrain objectives with a large working distance allowed to focus and then to collect the transmitted radiation, finally detected by a liquid-helium-cooled bolometer detector.

Raman and photoluminescence measurements at ambient conditions were carried out on $Mo_{0.5}W_{0.5}S_2$, MoS_2 and WS_2, using a Horiba LabRAM HR Evolution microspectrometer, with a 532 nm laser as light source. The radiation was focused on a 2 μm^2 spot on the sample by a 100x objective and collected by a CCD detector. Further details are provided in Ref.[37]

Results and discussion

Vibrational modes at ambient conditions

Infrared transmission measurements at ambient conditions were performed on $Mo_{0.5}W_{0.5}S_2$, WS_2, and MoS_2 crystals in the 100÷600 cm^{-1} range. To reduce the interference effects between the sample surfaces, each crystal was exfoliated on a diamond window, thus minimizing the discontinuity of the refractive index at the substrate interface. Measurements of the background intensity, $I_0(\omega)$, were preliminarily carried out on the bare diamond. The sample transmitted intensity, $I(\omega)$, was then measured once the crystals were positioned on the diamond, allowing to determine the absorbance spectra $A(\omega) = -ln[I(\omega)/I_0(\omega)]$. Raman measurements were also collected in the same frequency range as a reference. The comparison between absorbance and Raman spectra of $Mo_{0.5}W_{0.5}S_2$, WS_2, and MoS_2 is shown in Figure 1.

The absorbance spectrum of $Mo_{0.5}W_{0.5}S_2$ is characterized by the presence of four distinct bands between 300 cm^{-1} and 450 cm^{-1}. By comparing it with the $A(\omega)$ spectra of WS_2 and MoS_2, the peaks at $\sim$ 350 cm^{-1} and $\sim$ 380 cm^{-1} can be assigned to the E_{1u}-WS_2-like and the E_{1u}-MoS_2-like modes, respectively.[38,39] The larger bandwidth observed for the alloy peaks can be attributed to disorder effects, which are less important in the binary crystals. It is interesting to notice that, although Mo and W atoms are present in the sample with the same percentage, the intensity of E_{1u}-MoS_2-like is far larger than that of E_{1u}-WS_2-like. We recall that the infrared phonon intensity is proportional to the square of the first derivative of the dipole moment with respect to the normal mode coordinates. The dipole moment is related to the Born effective charge tensor, i.e. the first derivative of the polarization per unit cell with respect to the atomic displacements. Based on the Density Functional Theory calculations reported in the literature,[40] the Born charges (defined as one-third of the trace of the tensor in Cartesian coordinates) of Mo and W, for in-plane displacements, are in a 2:1 ratio, suggesting a four-times higher intensity of MoS_2-like mode compared with WS_2-like

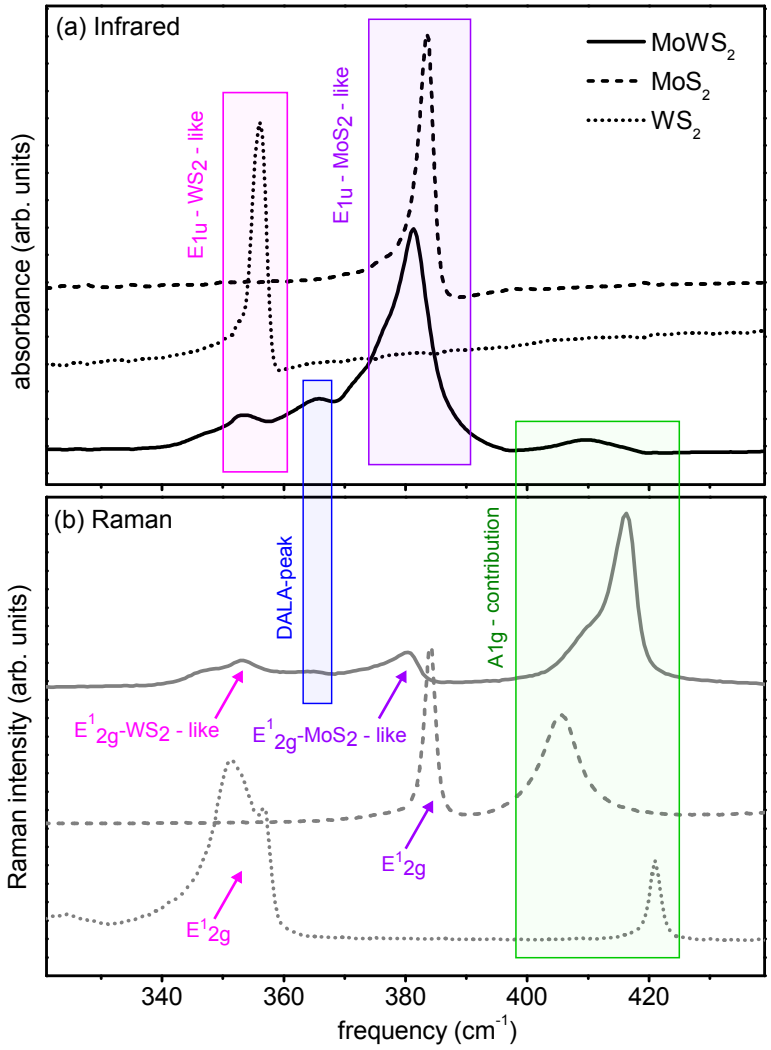

Figure 1: Infrared (a) and Raman (b) spectra of $Mo_{0.5}W_{0.5}S_2$ (continuous lines), MoS_2 (dashed lines), and WS_2 (dotted lines). Magenta and purple areas highlight the contributions of $Mo_{0.5}W_{0.5}S_2$ coming from the IR-active phonons of MoS_2 and WS_2 (E_{1u}). Blue and green areas highlight the contributions of $Mo_{0.5}W_{0.5}S_2$ coming from the IR-inactive, disorder-activated modes of MoS_2 and WS_2 (A_{1g}, DALA, see text).

one. The less intense peak at ~ 365 cm^{-1} between the two E_{1u} phonons may correspond to the disorder-activated longitudinal acoustic (DALA) phonon mode,[33] while the broad band at ~ 410 cm^{-1} could be identified with the convoluted A_{1g} modes from MoS_2 and WS_2.[24] Interestingly, both the DALA and the A_{1g}-like modes, whose symmetries are not compatible with the infrared selection rules, do not appear in the binary crystals but can be activated by disorder effects in the ternary compound.

Vibrational modes under high pressure

Room temperature transmission measurements on a $Mo_{0.5}W_{0.5}S_2$ single crystal were performed in the $100 \div 600$ cm^{-1} range, on increasing pressure from 0 to 31 GPa. The background intensity, $I_0(\omega)$, was measured with the DAC filled by the hydrostatic medium (CsI) only. The sample transmitted intensity, $I(\omega)$, was then collected once the crystal was loaded into the cell, to obtain the absorbance, $A(\omega)$, at each pressure. Interference fringes due to multiple reflections between the diamond surfaces through the hydrostatic medium were observed in $A(\omega)$ spectra. The reduced number of oscillations and the frequency dependence of both the period and the amplitude of the oscillations prevent an effective subtraction in the spectra.

The absorbance spectra on increasing pressure in the $350 \div 430$ cm^{-1} range, where the phonon contribution is dominant, are shown in Figure 2. Although the overall intensity of the peaks is reduced with respect to the out-of-cell measurements, a comparison with the spectra reported in Figure 1 allows identifying the principal bands associated with E_{1u}-WS_2-like (~ 350 cm^{-1}), DALA (~ 370 cm^{-1}), and E_{1u}-MoS_2-like (~ 380 cm^{-1}) vibrational modes. In the cell measurements, the A_{1g}-like contributions, visible at ambient conditions at ~ 410 cm^{-1}, are probably hindered by the interference fringes. Notice that, due to the alloyed nature of the compound, the relative intensity of the peaks may slightly vary depending on the measured point of the sample. In particular, disorder activated modes may be favoured in regions where the crystal order is reduced. By comparing Figures 1 and 2, the relative

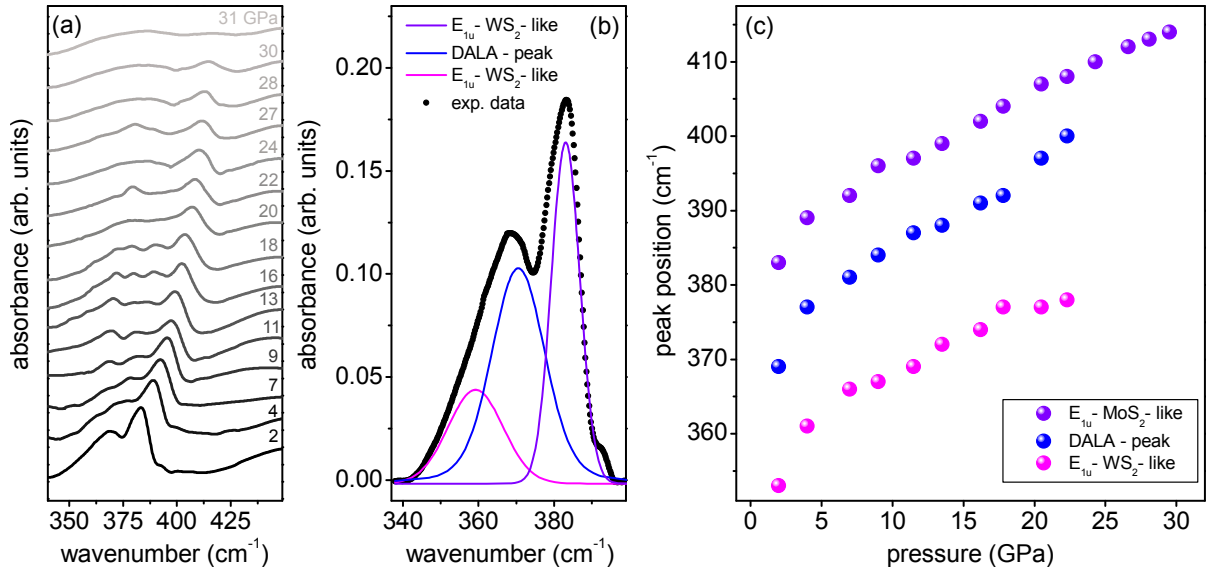

Figure 2: (a) Absorbance spectra of $Mo_{0.5}W_{0.5}S_2$ at increasing pressure from 2 to 31 GPa. Spectra are vertically shifted for sake of clarity. (b) Experimental phonon-peaks at 2 GPa (black dots) fitted with a sum of three Voigt functions. (c) g

intensity of the DALA mode is higher in the first case than in the second one. Since the investigated samples and the regions of the sample surface are different for in-cell- and out-of-cell-measurements, this effect can be ascribed to a different impact of configurational disorder.

As the pressure increases up to 31 GPa, the peak positions regularly shift toward higher frequencies, confirming the absence of structural transitions, as already suggested by Raman measurements.[33] The peak intensities above $\sim$ 20 GPa undergo a progressive lowering until completely vanishing at 31 GPa.

Electronic properties at ambient conditions

Thin $Mo_{0.5}W_{0.5}S_2$ crystals, mechanically exfoliated on a SiO_2-coated Si substrate, were analyzed through micro-Raman measurements to determine the number of layers (N) of each flake (see Supporting Information, SI). Photoluminescence (PL) measurements at ambient conditions were then performed to characterize the electronic properties of the sample as a function of N. PL spectra for mono-, bi-, tri- and four-layer samples are reported in Figure

3. The energy of the PL bands in the bulk sample is identical to that of the 4-layers sample, although the overall intensity is significantly lower. The spectrum of multi-layers samples exhibits three distinct bands: the one at lower energy ($\sim 1.4 \div 1.5$ eV) corresponds to the exciton associated with the indirect-gap transition, the most intense one at ~ 1.85 eV, is the A exciton, and the one at ~ 2.1 eV is the B exciton, the latter two related to direct transitions.[41] The energy difference between the peaks associated with A and B excitons corresponds to the spin-orbit splitting of the valence band of the crystal. In the mono-layer, the well-known transition from indirect to direct gap occurs, and the indirect transition band is no longer visible in the spectrum.

The comparison between the PL spectra of $Mo_{0.5}W_{0.5}S_2$, MoS_2, and WS_2 (see SI) clearly shows that all the electronic features of the ternary compound lie at halfway between its basic constituents. In particular, in the bulk sample, we measured an indirect gap of ~ 1.4 eV, a direct gap of ~ 1.85 eV, and a spin-orbit splitting of ~ 0.29 eV.[41] Indeed, as widely demonstrated in the literature,[21] the optical band-gap of alloyed crystals strongly depends on the Mo/W ratios and continuously tunable band-gap can be achieved by controlling the percentage of transition metal atoms in the sample.

Electronic properties under high-pressure

To study the evolution of the electronic properties of $Mo_{0.5}W_{0.5}S_2$ as a function of pressure, we analyzed the spectral weight in the far-infrared range at increasing pressure values. This quantity indeed accounts for the low-energy electronic transitions and, thus, allows to monitor a possible insurgence of the metallic regime.

As shown in Figure 4(a), the $A(\omega)$ spectra in the FIR region are almost superimposed up to ~ 18 GPa. On further increasing pressure, the overall absorption intensity rises and the phonon peak intensity reduces. The first effect may arise from a rapid increase of the free electron density, due to the insurgence of a Drude band at zero frequency. Indeed, as in most semiconducting TMDs, in $Mo_{0.5}W_{0.5}S_2$ the high pressure reasonably drives a pro-

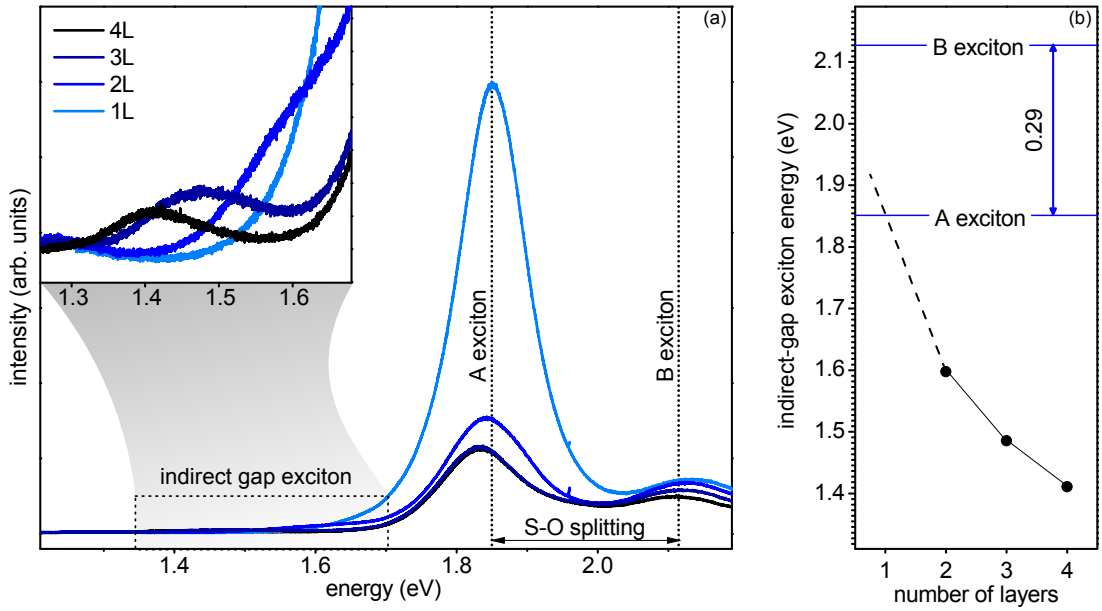

Figure 3: (a) PL spectrum of $Mo_{0.5}W_{0.5}S_2$ samples with a different number of layers. (b) Energy of the exciton associated with the indirect gap as a function of the number of layers.

gressive reduction of the band-gap responsible for the semiconductor-to-metal transition. Correspondingly, the intensity of the vibrational modes decreases since the optical response of the free electrons shields the phonon contribution in the FIR absorption.

To quantitatively characterize the metallization process, we define at each pressure the absorption spectral weight $sw(P) = \int_{\omega_m}^{\omega_M} A(\omega)d\omega$.[42,43] A simple application of the Drude model proves that in the low-frequency limit, i.e. $\omega/\Gamma \ll 1$ (whit $\Gamma = c/\tau$ and τ the Drude relaxation time), the absorbance is simply proportional to the square root of the DC conductivity σ_0 and ω, $A(\omega) \propto \sqrt{\sigma_0 \omega}$. Since σ_0 is proportional to the carrier density n, the last relation demonstrates that the increase in the FIR absorbance is directly related to the increase of n.[44,45] Figure 4(b) reports the values of the normalized spectral weight $SW(P, P_0) = sw(P)/sw(P_0)$ up to 31 GPa, where $P_0 = 2$ GPa and the integration limits are ω_m=200 cm^{-1} and ω_M=700 cm^{-1}. The integration is not performed over the 350÷450 cm^{-1} range where the phonon contribution is predominant. The normalized spectral weight, almost constant at low pressure, undergoes a significant increase around $\sim$ 20 GPa, associ-

ated to an increase of the charge carrier density n. To identify the onset of the metallization process, two independent linear fits were performed in the 2÷20 GPa and the 16÷31 GPa ranges (see Figure 3(b)): the ordinate of the crossing point of fitting lines, $P_M = 18 \pm 1$ GPa, could be assumed as a reference pressure value to describe the beginning of the metallic transition, where actually a strong increase of the spectral weight occurs.[46] It is worth to underline that P_M reasonably underestimates the effective metallization pressure by a few GPa. Indeed, the increase in the charge carrier density might arise when the band gap is not completely closed but is reduced down to $\sim k_B T$, allowing the electrons in the valence band to be thermally promoted in the conduction band.

The obtained results display a very good agreement with the theoretical calculations reported in the literature[34] that predicted a semiconductor-to-metal transition above 20 GPa for bulk $Mo_{0.5}W_{0.5}S_2$. They are also well compatible with previous high-pressure measurements at room temperature on MoS_2 and WS_2, which have shown a metallic transition between 19 and 22 GPa for both samples.[27,28] Interestingly, in the $Mo_{0.5}W_{0.5}S_2$ alloy the substitutional disorder of the crystal lattice, attested by the presence of the disorder-activated phonon peaks, does not strongly affect the electronic properties of the sample.

Conclusion

Transmission measurements were performed on a $Mo_{0.5}W_{0.5}S_2$ single crystal in the far-infrared range. The spectrum collected at ambient conditions enabled the classification of the observed peaks in terms of the lattice vibrational modes, by comparison with the spectra of the binary constituents MoS_2 and WS_2. High-pressure measurements allowed us to study the evolution of the lattice dynamics and to estimate the trend of the free carrier density up to 31 GPa. The behaviour of the phonon peaks under pressure, well compatible with the Raman measurements reported in the literature,[33] confirms the absence of structural transitions in the considered pressure range, while the abrupt increase of the spectral

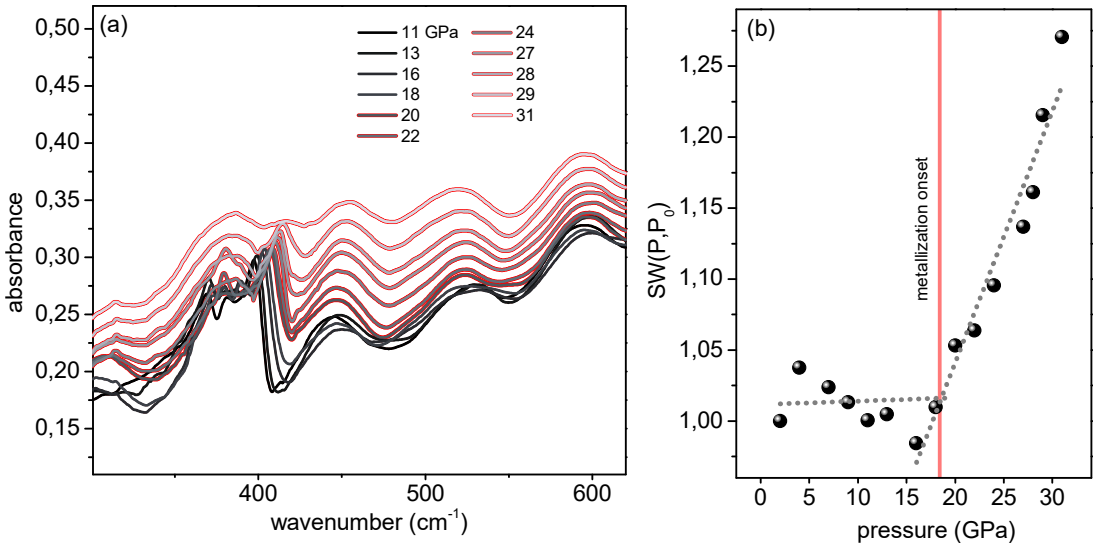

Figure 4: (a) Absorbance spectra of $Mo_{0.5}W_{0.5}S_2$ from 11 GPa to 31 GPa. Above 20 GPa, spectra with a red contour are characterized by increasing spectral weight. (b) Normalized spectral weight ($SW(P,P_0)$) as a function of pressure. Linear fits in the 2÷20 GPa and the 16÷31 GPa ranges are reported as dotted lines.

weight above 18 GPa seems to indicate an increase of the charge carrier density. These results suggested the occurrence of an isostructural transition from a semiconducting to a metallic state in $Mo_{0.5}W_{0.5}S_2$ never experimentally investigated before in the literature. These results suggest the occurrence of an isostructural transition from a semiconducting to a metallic state in bulk $Mo_{0.5}W_{0.5}S_2$ in very good agreement with the theoretical calculations reported in the literature,[34] which predicted the onset of the metallization process above 20 GPa. The observed effect is also coherent with previous studies on the binary compounds that found out a metallization pressure of $\sim$ 19 GPa[27] and $\sim$ 22 GPa[28] for MoS_2 and WS_2 respectively, without relevant changes in the lattice symmetries. The compatibility between the metallization pressures of $Mo_{0.5}W_{0.5}S_2$ and its constituents suggests that substitutional disorder does not play a key role in the evolution of the electronic properties of the alloy under pressure.

Supporting Information: Raman measurements on $Mo_{0.5}W_{0.5}S_2$; photoluminescence measurements on MoS_2 and WS_2.

Acknowledgements

We acknowledge SOLEIL for provision of synchrotron radiation facilities and we would like to thank Dr. Anna Celeste and Dr. Bordondis Ferenc for assistance in using beamline SMIS.

References

(1) Yuan, L.; Ge, J.; Peng, X.; Zhang, Q.; Wu, Z.; Jian, Y.; Xiong, X.; Yin, H.; Han, J. A reliable way of mechanical exfoliation of large scale two dimensional materials with high quality. *AIP Adv.* **2016**, *6*, 125201.

(2) Manzeli, S.; Ovchinnikov, D.; Pasquier, D.; Yazyev, O. V.; Kis, A. 2D transition metal dichalcogenides. *Nature Reviews Materials* **2017**, *2*, 17033.

(3) Peng, J.; Wu, J.; Li, X.; Zhou, Y.; Yu, Z.; Guo, Y.; Wu, J.; Lin, Y.; Li, Z.; Xiaojun Wu, e. a. Very Large-Sized Transition Metal Dichalcogenides Monolayers from Fast Exfoliation by Manual Shaking. *Journal of the American Chemical Society* **2017**, *139*, 9019–9025.

(4) Li, X.; Tao, L.; Chen, Z.; Fang, H.; Li, X.; Wang, X.; Xu, J. B.; Zhu, H. Graphene and related two-dimensional materials: Structure-property relationships for electronics and optoelectronics. *App. Phys. Rev.* **2017**, *4*, 021306.

(5) Wang, Q. H.; Kalantar-Zadeh, K.; Kis, A.; Coleman, J. N.; Strano, M. S. Electronics and optoelectronics of two-dimensional transition metal dichalcogenides. *Nature Nanotechnology* **2012**, *7*, 699–712.

(6) Jariwala, D.; Sangwan, V. K.; Lauhon, L. J.; Marks, T. J.; Hersam, M. C. Emerging Device Applications for Semiconducting Two-Dimensional Transition Metal Dichalcogenides. *ACS Nano* **2014**, *8*, 1102–1120.

(7) Lu, C.; Chen, C. Structure-strength relations of distinct MoN phases from first-principles calculations. *Phys. Rev. Materials* **2020**, *4*, 044002.

(8) Lu, C.; Chen, C. Indentation-strain stiffening in tungsten nitrides: Mechanisms and implications. *Phys. Rev. Materials* **2020**, *4*, 043402.

(9) Heiße, F.; Köhler-Langes, F.; Rau, S.; Hou, J.; Junck, S.; Kracke, A.; Mooser, A.; Quint, W.; Ulmer, S.; Werth, e. a. High-Precision Measurement of the Proton's Atomic Mass. *Phys. Rev. Lett.* **2017**, *119*, 033001.

(10) Yun, W. S.; Han, S. W.; Hong, I. G., S. C.and Kim; Lee, J. D. Thickness and strain effects on electronic structures of transition metal dichalcogenides: 2H-MX_2 semiconductors (M = Mo, W; X = S, Se, Te). *Phys. Rev. B* **2012**, *85*, 033305.

(11) Mak, K. F.; Lee, C.; Hone, J.; Shan, J.; Heinz, T. F. Atomically Thin MoS_2: A New Direct-Gap Semiconductor. *Phys. Rev. Lett.* **2010**, *105*, 136805.

(12) y. Zhang et al., Direct observation of the transition from indirect to direct bandgap in atomically thin epitaxial $MoSe_2$. *Nat. Nanotechnol.* **2013**, *9*, 111âĂŞ115.

(13) Xie, L. M. Two-dimensional transition metal dichalcogenide alloys: preparation, characterization and applications. *Nanoscale* **2015**, *7*, 18392–18401.

(14) Zhao, Y.; Zhang, Z.; Ouyang, G. Band shift of 2D transition-metal dichalcogenide alloys: size and composition effects. *Applied Physics A* **2018**, *124*, 292.

(15) Sahoo, S.; Gaur, A. P. S.; Ahmadi, M.; Guinel, M. J.-F.; Katiyar, R. S. Temperature-Dependent Raman Studies and Thermal Conductivity of Few-Layer MoS2. *The Journal of Physical Chemistry C* **2013**, *117*, 9042–9047.

(16) Chakraborty, B.; Matte, H. S. S. R.; Sood, A. K.; Rao, C. N. R. Layer-dependent resonant Raman scattering of a few layer MoS2. *Journal of Raman Spectroscopy* **2012**, *44*, 92–96.

(17) Mahatha, S. K.; Patel, K. D.; Menon, K. S. R. Electronic structure investigation of MoS2and MoSe2using angle-resolved photoemission spectroscopy andab initioband structure studies. *Journal of Physics: Condensed Matter* **2012**, *24*, 475504.

(18) Ulstrup, S.; Čabo, A. G. c. v. a. c.; Biswas, D.; Riley, J. M.; Dendzik, M.; Sanders, C. E.; Bianchi, M.; Cacho, C.; Matselyukh, D.; Chapman, e. a., Richard T. Spin and valley control of free carriers in single-layer WS_2. *Phys. Rev. B* **2017**, *95*, 041405.

(19) Sekine, T.; Nakashizu, T.; Toyoda, K.; Uchinokura, K.; Matsuura, E. Raman scattering in layered compound 2H-WS2. *Solid State Communications* **1980**, *35*, 371–373.

(20) Carvalho, B. R.; Malard, L. M.; Alves, J. M.; Fantini, C.; Pimenta, M. A. Erratum: Symmetry-Dependent Exciton-Phonon Coupling in 2D and Bulk MoS_2 Observed by Resonance Raman Scattering [Phys. Rev. Lett. 114, 136403 (2015)]. *Phys. Rev. Lett.* **2016**, *116*, 089904.

(21) Wang, Z.; Liu, P.; Ito, Y.; Ning, S.; Tan, Y.; Fujita, T.; Hirata, A.; Chen, M. Chemical Vapor Deposition of Monolayer Mo1-xWxS2 Crystals with Tunable Band Gaps. *Scientific Reports* **2016**, *6*, 21536.

(22) Kim, J.-S.; Ahmad, R.; Pandey, T.; Rai, A.; Feng, S.; Yang, J.; Lin, Z.; Terrones, M.; Banerjee, S. K.; et al., A. K. S. Towards band structure and band offset engineering of monolayer $Mo_xW_{1-x}S_2$ via Strain. *2D Materials* **2017**, *5*, 015008.

(23) Qiao, X.-F.; Li, X.-L.; Zhang, X.; Shi, W.; Wu, J.-B.; Chen, T.; Tan, P.-H. Substrate-free layer-number identification of two-dimensional materials: A case of Mo0.5W0.5S2 alloy. *Applied Physics Letters* **2015**, *106*, 223102.

(24) Zhang, X.; Qiao, X.-F.; Shi, W.; Wu, J.-B.; Jiang, D.-S.; Tan, P.-H. Phonon and Raman scattering of two-dimensional transition metal dichalcogenides from monolayer, multilayer to bulk material. *Chem. Soc. Rev.* **2015**, *44*, 2757–2785.

(25) Stellino, E. Pressure evolution of the optical phonons of MoTe2. *Il Nuovo Cimento C* **2020**, *43*, 1âĂŞ8.

(26) Yang, L.; Dai, L.; Li, H.; Hu, H.; Liu, K.; Pu, C.; Hong, M.; Liu, P. Pressure-induced metallization in MoSe2 under different pressure conditions. *RSC Advances* **2019**, *9*, 5794–5803.

(27) Nayak, A. P.; Bhattacharyya, S.; Zhu, J.; Liu, J.; Wu, X.; Pandey, T.; Jin, C.; Singh, A. K.; Akinwande, D.; Lin, J.-F. Pressure-induced semiconducting to metallic transition in multilayered molybdenum disulphide. *Nature Communications* **2014**, *5*, 3731.

(28) Nayak, A. P.; Yuan, Z.; Cao, B.; Liu, J.; Wu, J.; Moran, S. T.; Li, T.; Akinwande, D.; Jin, C.; Lin, J.-F. Pressure-Modulated Conductivity, Carrier Density, and Mobility of Multilayered Tungsten Disulfide. *ACS Nano* **2015**, *9*, 9117–9123.

(29) **2010**, *81*, 195209.

(30) Livneh, T.; Reparaz, J. S.; Goñi, A. R. Low-temperature resonant Raman asymmetry in 2H-MoS2 under high pressure. *Journal of Physics: Condensed Matter* **2017**, *29*, 435702.

(31) Brotons-Gisbert, M.; Segura, A.; Robles, R.; Canadell, E.; Ordejón, P.; Sánchez-Royo, J. F. Optical and electronic properties of 2H$-MoS_2$ under pressure: Revealing the spin-polarized nature of bulk electronic bands. *Phys. Rev. Materials* **2018**, *2*, 054602.

(32) Zhuang, Y.; Dai, L.; Wu, L.; Li, H.; Hu, H.; Liu, K.; Yang, L.; Pu, C. Pressure-induced permanent metallization with reversible structural transition in molybdenum disulfide. *Applied Physics Letters* **2017**, *110*, 122103.

(33) Kim, J.-S.; Moran, S. T.; Nayak, A. P.; Pedahzur, S.; Ruiz, I.; Ponce, G.; Rodriguez, D.; Henny, J.; Liu, J.; Lin, J.-F.; Akinwande, D. High pressure Raman study of layered $Mo_{0.5}W_{0.5}S_2$ ternary compound. *2D Materials* **2016**, *3*, 025003.

(34) Jiansheng, D.; Gang, O. Thickness-Dependent Semiconductor-to-Metal Transition in Molybdenum Tungsten Disulfide Alloy under Hydrostatic Pressure. *ACS Omega* **2019**, *4*, 8641 âĹŠ 8649.

(35) Celeste, A.; Borondics, F.; Capitani, F. Hydrostaticity of pressure-transmitting media for high pressure infrared spectroscopy. *High Pressure Research* **2019**, *39*, 608–618.

(36) Chijioke, A. D.; Nellis, W. J.; Soldatov, A.; Silvera, I. F. The ruby pressure standard to 150GPa. *Journal of Applied Physics* **2005**, *98*, 114905.

(37) Caramazza, S.; Collina, A.; Stellino, E.; Ripanti, F.; Dore, P.; Postorino, P. First-and second-order Raman scattering from MoTe 2 single crystal. *The European Physical Journal B* **2018**, *91*, 1–7.

(38) O'Neal, K. R.; Cherian, J. G.; Zak, A.; Tenne, R.; Liu, Z.; Musfeldt, J. L. High Pressure Vibrational Properties of WS2 Nanotubes. *Nano Letters* **2016**, *16*, 993–999.

(39) Guo, X.; Chen, H.; Wen, X.; Zheng, J. Electron-phonon interactions in MoS2 probed with ultrafast two-dimensional visible/far-infrared spectroscopy. *The Journal of Chemical Physics* **2015**, *142*, 212447.

(40) Pike, N. A.; Van Troeye, B.; Dewandre, A.; Petretto, G.; Gonze, X.; Rignanese, G.-M.; Verstraete, M. J. Origin of the counterintuitive dynamic charge in the transition metal dichalcogenides. *Phys. Rev. B* **2017**, *95*, 201106.

(41) Chen, Y.; Xi, J.; Dumcenco, D. O.; Liu, Z.; Suenaga, K.; Wang, D.; Shuai, Z.; Huang, Y.-S.; Xie, L. Tunable Band Gap Photoluminescence from Atomically Thin Transition-Metal Dichalcogenide Alloys. *ACS Nano* **2013**, *7*, 4610–4616.

(42) Arcangeletti, E.; Baldassarre, L.; Di Castro, D.; Lupi, S.; Malavasi, L.; Marini, C.; Perucchi, A.; Postorino, P. Evidence of a Pressure-Induced Metallization Process in Monoclinic VO_2. *Phys. Rev. Lett.* **2007**, *98*, 196406.

(43) Dore, P.; Sacchetti, A.; Postorino, P.; Congeduti, A.; Gorelli, F. A.; Ulivi, L. Evidence of Phase Separation in the P-T Phase Diagram of the La0.75Ca0.25MnO3 Manganite by Infrared Measurements. *Journal of Superconductivity* **2005**, *18*, 659–662.

(44) Postorino, P.; Congeduti, A.; Dore, P.; Sacchetti, A.; Gorelli, F.; Ulivi, L.; Kumar, A.; Sarma, D. D. Pressure Tuning of Electron-Phonon Coupling: The Insulator to Metal Transition in Manganites. *Physical Review Letters* **2003**, *91*, 175501.

(45) Calvani, P.; Marzi, G. D.; Dore, P.; Lupi, S.; Maselli, P.; D'Amore, F.; Gagliardi, S.; Cheong, S.-W. Infrared Absorption from Charge Density Waves in Magnetic Manganites. *Physical Review Letters* **1998**, *81*, 4504–4507.

(46) Liang, Y.; Huang, X.; Huang, Y.; Wang, X.; Li, F.; Wang, Y.; Tian, F.; Liu, B.; Shen, Z. X.; Cui, T. New Metallic Ordered Phase of Perovskite $CsPbI_3$ under Pressure. *Advanced Science* **2019**, *6*, 1900399.

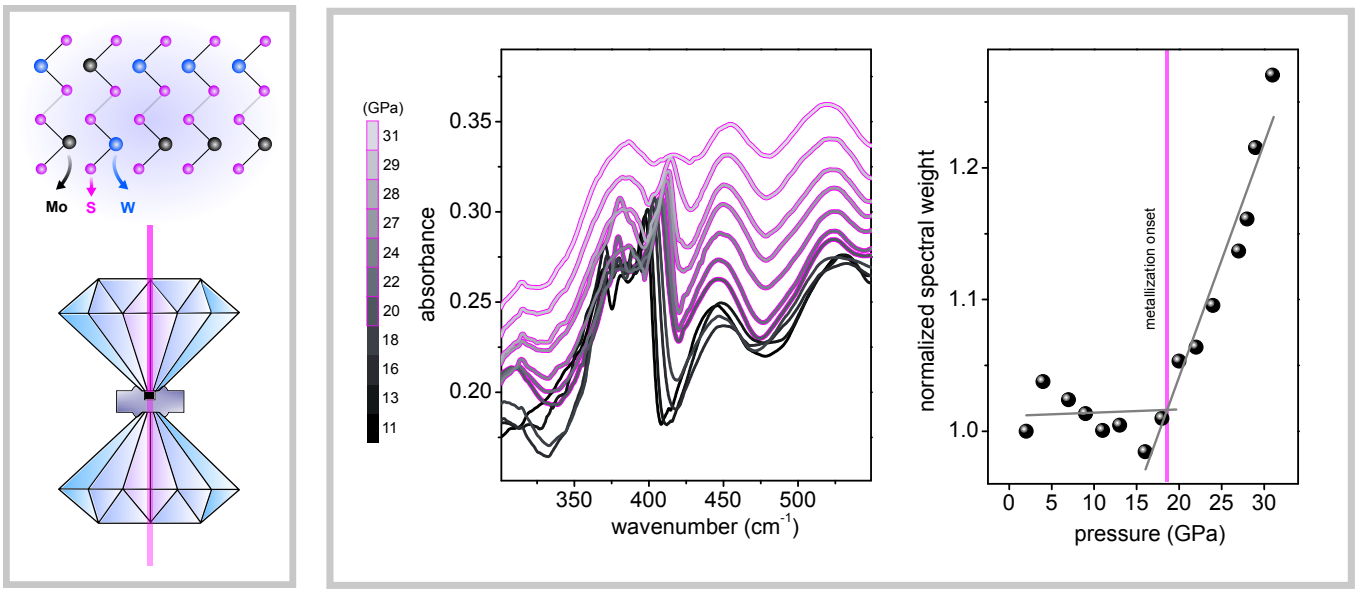

Figure 5: Graphical Abstract